Nationaal Lucht- en Ruimtevaartlaboratorium
National Aerospace Laboratory NLR

Executive summary

Gas turbine combustor liner life assessment using a fluid / structural approach

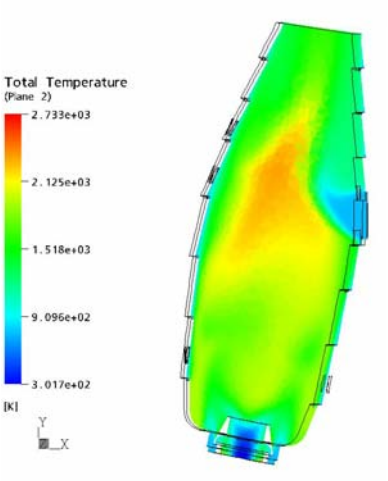

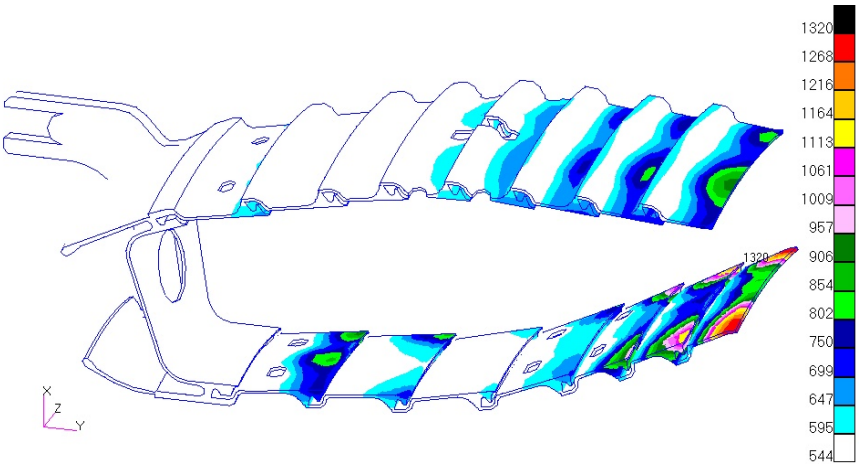

Problem area
In recent years NLR has developed lifing tools for gas turbine components. These tools are used to assist gas turbine operators with usage and maintenance. Models for HP and LP turbine blades and compressor and turbine discs are now available and can be applied. One of the missing links in the method is a model for combustion chambers. This paper describes the development of a combustor liner lifing method.

Description of the work
Since the loading of a combustor liner is mainly thermal, the combustion process must be modeled to obtain the proper input for a finite element (FE) analysis. The NLR has no experience in this field and therefore a collaboration with the Laboratory of Thermal Engineering at Twente University (UT) was set up.

At the UT, Computational Fluid Dynamics (CFD) analyses were performed on the combustion process to predict the thermal loading of the liner. These results were used as input for the NLR FE analyses. The temperature distribution in the liner wall was calculated for several (steady-state) operating conditions. Then the resulting deformations and stresses were determined and finally a life assessment was performed. In this lifing analysis both creep and thermal fatigue were taken into account.

Also a method was developed to efficiently analyze a complete

Report no.
NLR-TP-2005-627

Author(s)
T. Tinga, J.F. van Kampen,
B. de Jager and J.B.W. Kok

Report classification
unclassified

Date
December 2005

Knowledge area(s)
Gas Turbine Technology
Comptational Mechanics & Simulation Technology
Aerospace Collaborative Engineering & Design

Descriptor(s)
Combustion chambers
Finite Element method
Service Life
Fatigue Life
Creep analysis

flight. CFD analyses are computationally very expensive and can therefore not be performed for any condition that occurs during a flight. Hence, CFD analyses were performed for a limited number of conditions and interpolation between these conditions yielded the results for any other condition.

Results and conclusions
The thermal loading of the combustor liner was calculated for a complete measured flight, and a life assessment was performed. The results were compared to field experience, which showed that the location and growth direction of cracks could be predicted quite well. However, prediction of the actual service life of the liner appeared to be hard due to the lack of experimental data to tune the model.

Applicability
The developed method can be applied to perform sensitivity analyses and comparative studies on combustor liners, e.g. to study the qualitative effect of different mission types on life consumption.

Nationaal Lucht- en Ruimtevaartlaboratorium, National Aerospace Laboratory NLR

Anthony Fokkerweg 2, 1059 CM Amsterdam,
P.O. Box 90502, 1006 BM Amsterdam, The Netherlands
Telephone +31 20 511 31 13, Fax +31 20 511 32 10, Web site: www.nlr.nl

Nationaal Lucht- en Ruimtevaartlaboratorium
National Aerospace Laboratory NLR

NLR-TP-2005-627

Gas turbine combustor liner life assessment using a fluid / structural approach

T. Tinga, J.F. van Kampen*, B. de Jager* and J.B.W. Kok*

* Twente University

This report has been based on a paper submitted to the ASME Journal of Engineering for Gas Turbines and Power.

Customer:	National Aerospace Laboratory NLR
Working Plan number:	AV.1.B
Owner:	National Aerospace Laboratory NLR
Division:	Aerospace Vehicles
Distribution:	Unlimited
Classification title:	Unclassified
	November 2005

Approved by:

Author	Reviewer	Managing department
20/12	19-12-2005	21/12

Summary

This report contains a paper that was submitted to the ASME Journal of Engineering for Gas Turbines and Power. A summary of the contents can be found in the abstract of the paper.

Contents

(30 pages in total)

Gas turbine combustor liner life assessment using a combined fluid/structural approach

T. Tinga[*], J.F. van Kampen[$], B. de Jager[$], J.B.W. Kok[$],

[*] *National Aerospace Laboratory NLR, Anthony Fokkerweg 2, 1059 CM, Amsterdam, The Netherlands, Tel.: +31-527-248727, fax: +31-527-248210, email: tinga@nlr.nl*

[$] *Twente University, Thermal Engineering, P.O. Box 217, 7500 AE Enschede, The Netherlands*

Abstract

A life assessment was performed on a fighter jet engine annular combustor liner, using a combined fluid / structural approach. Computational fluid dynamics analyses were performed to obtain the thermal loading of the combustor liner and finite element analyses were done to calculate the temperature and stress/strain distribution in the liner during several operating conditions. A method was developed to analyze a complete flight with limited computational effort. Finally the creep and fatigue life for a measured flight were calculated and the results were compared to field experience data. The absolute number of cycles to crack initiation appeared hard to predict, but the location and direction of cracking could be correlated well with field data.

Keywords: Computational fluid dynamics; heat transfer; finite element; combustor; life assessment

1 Introduction

To improve gas turbine efficiency the operating temperatures have steadily increased. This makes greater demands on the structural integrity of the gas turbine components, especially the turbine blades and vanes and the combustor liner. The ability to perform a reliable life assessment is crucial for both gas turbine component design and maintenance. Damage as is shown for a combustor liner in Figure 1 must be detected and repaired before it gets problematic. Therefore, reliable determination of inspection intervals is very important. To achieve this a vast amount of research has been done on predicting the time dependent thermo-mechanical loading of gas turbine components and performing life assessments.

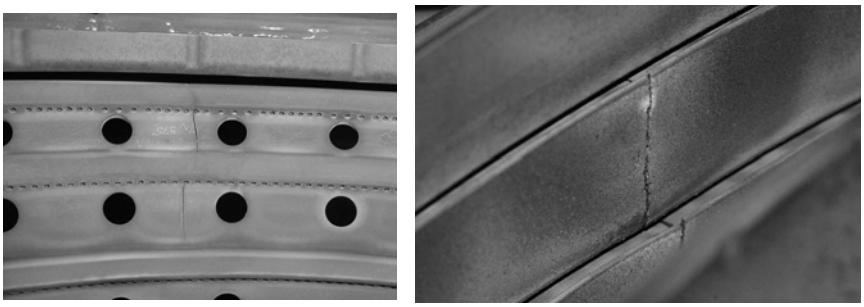

Figure 1 Cracks in inner and outer liner of combustor.

The majority of the work published so far is devoted to turbine blades, since the high rotational speeds make these components the most severely loaded gas turbine components. The scope of the published work ranges from relatively simple engineering approaches [1],[2] towards integrated multidisciplinary approaches combining computational fluid dynamics (CFD) and finite element (FE) codes to perform life assessments [3]. Surprisingly, much less work has been done on assessing the life of combustor liners.

The literature on combustors is mainly focussed on fluid dynamics and combustion process optimization aiming at reducing emissions or optimizing the turbine inlet temperature profile [4] - [9]. The amount of published work on the prediction of liner thermal loading is very limited. Lai [10] did some work in this field and used a computational fluid dynamics analysis to predict the location of hot spots on a combustor liner. Also the amount of publications on the coupling between the fluid and structural disciplines and on combustor life assessment is very limited. One of the few contributions in this field is the paper by Kiewel [11] that treats the life assessment of a ring combustor. In this work a measured temperature distribution at a single operating condition was used in stead of a CFD calculated thermal loading history.

In the present work the integrated methods used for turbine blades were extended towards combustor liners. Mainly two developments were made to achieve this. Firstly a connection was established between several disciplines to be able to perform an integrated life assessment. Secondly a method was developed to analyse a complete measured aircraft flight.

In the next section the different constituents of this multidisciplinary approach are described. Then section 3 describes the method developed to analyse a real flight. In section 4 the results are presented and finally section 5 contains the conclusions.

2 Multidisciplinary approach

Based on the output of an engine performance simulation program a CFD analysis was performed to simulate the combustion process and to calculate the liner thermal loading. Then a finite element analysis was used to predict the liner temperature and stress distribution, which were used as input for a life assessment. This section describes the details of the individual constituents of this integrated approach and their interfaces.

The engine system performance simulation program GSP [14] was used to calculate the input parameters for the CFD analyses. Measured engine and flight data, like power setting, altitude and speed, were used to simulate a real flight. GSP provided gas temperatures, pressures and mass flows at combustor entry and exit, which were used as boundary conditions in the CFD analyses.

The CFD model describes the behavior of the gas volume inside the combustor liner whereas the FE model describes the behavior of the structure (i.e. the liner) surrounding the gas. Since the loading of the structure is governed by the thermal and fluid dynamical behavior of the gas, it is very important that the geometry of the CFD and FE models matches at the interface through which they are coupled. Therefore the models were constructed from the same geometric model. This geometric model was constructed from technical drawings and handbooks, taking into account details like the location and dimension of dilution and boroscope holes. The combustor liner is shown in Figure 2 and the resulting CFD and FE models in Figure 3.

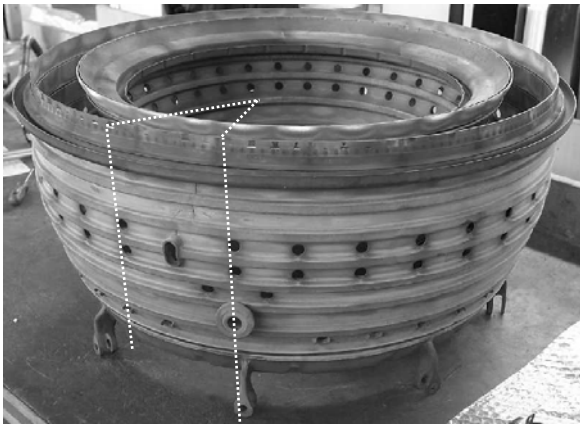

Figure 2 Combustor liner with 1/16th section that is modeled indicated by dotted line.

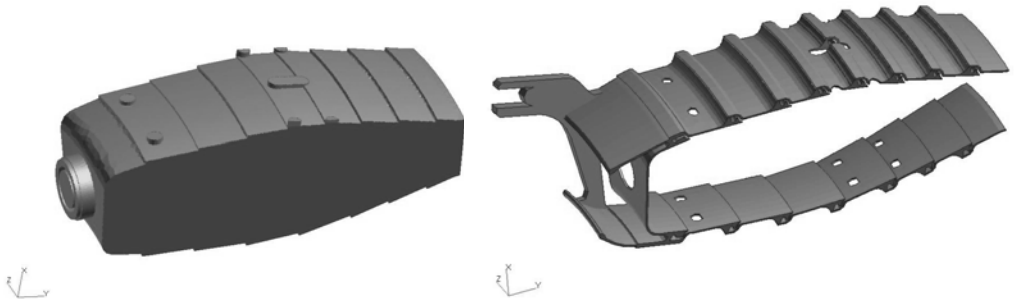

Figure 3 Geometry of CFD (left) and FE models (right).

As a result of the periodic flow field in the annular combustor, only 1/16th section of the total combustor had to be modelled. This is indicated by the dotted line in Figure 2. Only the distribution of the boroscope holes is not periodic as these holes are not present in all sections (only four). Since the effect of the holes on the flow behavior inside the liner was believed to be significant, a boroscope hole was modeled in the 1/16th section (see Figure 3).

2.1 Computational fluid dynamics model

A fluid-dynamical analysis of the combustor was performed using the commercial CFD code ANSYS CFX 5.7. This code uses an unstructured solver, which facilitates the meshing of the relatively difficult geometry of the combustor (see Figure 3). The geometry was meshed with mainly triangular mesh elements. The total number of elements assembling the geometry is 1.4 million.

In this section, the models that were used in the CFD analysis are described. Moreover, the translation step from the GSP data to boundary conditions for the CFD model is treated.

2.1.1 Model description

For all cases considered in this paper, the flow in the combustor is turbulent. To predict the effects of turbulence on flow, combustion and heat transfer, the standard available k-epsilon turbulence model was used. At all inlet boundaries, a turbulence intensity of 10% of the mean inlet velocities was assumed, corresponding to intense turbulence.

Combustion was accounted for by a single-step combustion model which uses an effective Arrhenius law for the reaction rate. The fuel was considered to be fully vaporised, i.e. no liquid phase is included in the simulation. The aero gas turbine hydrocarbon fuel JP10 was used, for which the Arrhenius constants were fitted from a Computational Singular Perturbation method based reduced version of a detailed chemical reaction scheme (see De Jager et al. [15] and

Appendix A JP10 jet fuel chemistry). From laminar flame data the reaction rate as a function of temperature is known. In order to establish the activation energy constant in an Arrhenius like relation for the global conversion of JP10 into combustion products, a Gaussian fit can be applied to this data. The Gaussian fit to the activation energy and the pre-exponential factor is given by:

$$S_\eta = 2610 e^{-\left(\frac{T-1938}{358.2}\right)} \; [kg/m^3/s] \qquad (1)$$

These fitted global rate constants can be used in a simple finite rate combustion simulation.
The flame in the combustor is stabilised by a recirculation zone of hot gases. This recirculation zone is the result of the swirling inlet flow. The axial swirler vanes of the burner were not included in the model. However, from the geometry of the actual axial swirler vanes, a 45 degree angle between the tangential and axial velocity was estimated. The swirlers of the burners in the annular combustor are co-rotating, which justifies the use of periodic boundary conditions at the radial planes bounding the model.
The influence of the combustor walls on the flow was modelled with a wall function. The walls itself were modelled as non-adiabatic walls. At the cooling air side of the walls (outside the computational domain), a heat transfer coefficient was imposed. This heat transfer coefficient was calculated from the Nusselt correlation of Dittus-Boelter. The input for this correlation followed from the geometry of the cooling passage and the total amount of air flowing past the inner and outer liner (see Figure 4). These mass flows were determined by an analysis of the air distribution over the combustor, which is treated in the next section. The different mass flows yielded different heat transfer coefficients for inner and outer liner, ranging from 140 to 1400 W/m^2K, depending on the engine operating condition considered. To obtain the heat flux to the cooling air, also the temperature of the cooling air was required, which was assumed to be constant. Since the residence time of the air in the cooling passage is in the order of a few milliseconds, the cooling air has only a small temperature increase while flowing past the liner.
Besides convective heat transfer, radiation was accounted for as well. The fluid was considered optically transparent, implying that only radiation from the fluid to the walls was included in the analysis. Additionally, the radiative heat loss from the liner to the casing was modelled. For this purpose, a constant temperature was assumed for the casing: 100 K below the cooling air temperature.

2.1.2 Boundary conditions

The GSP generated input data had to be transformed to mass flows at each inlet of the CFD model. These inlets comprise: the annular air swirler inlet of the burner, 7 film cooling inlets in the inner liner, 8 film cooling inlets in the outer liner, 3 pairs of dilution holes in the inner liner, 3 pairs of dilution holes in the outer liner and the boroscope hole in the outer liner (see Figure 4).

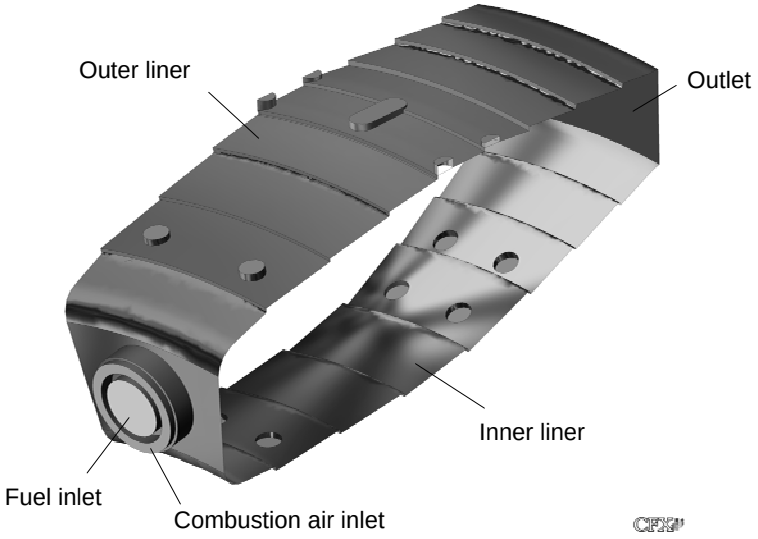

Figure 4 Inlets and outlet in CFD geometry

The film cooling holes, with a 1.5 mm diameter, are located in rows along the steps of the liner. For convenient modelling, the holes in each row were merged into a single slit-formed inlet. The pre-vaporised fuel was supplied at the centre of the burner mouth. Furthermore, the distribution of the air over the inlets was derived from the areas of each inlet. For this purpose, the pressure drop over each inlet was calculated with Bernoulli's law. Subsequently, the pressure drops over the inlets were matched in an iterative way. This approach is based on the assumption that a constant pressure can be assumed outside and around the combustor.

2.2 Finite Element model

The finite element analysis was performed using the commercial FE code MSC.Marc 2001. In the geometry as shown in Figure 3 a finite element mesh was created with isoparametric 8-node hexagonal elements. Typically ten elements were used in circumferential direction and two elements across the liner wall thickness, resulting in a total number of 11646 elements and 18285 nodes.

The model was first used for a thermal analysis to calculate the temperature distribution in the liner, using the CFD results as input. Then a structural analysis was performed to calculate the stress and strain distribution. The loads and boundary conditions that were used in these analyses are described in the next subsections.

2.2.1 Thermal analysis

During the combustion process heat is transferred from the flame to the liner walls by convection and radiation. At the same time, cooling at the other side of the liner causes heat transfer from the liner wall to the cooling gas. This causes a temperature gradient across the wall thickness. These processes have to be covered by the thermal analysis, using the CFD results as input. This was done in the following manner (see also Figure 5).

- prescribing the CFD calculated wall adjacent gas temperature and heat transfer coefficient at the inner wall of the liner (convective boundary condition, Q_{conv})
$$Q_{conv} = h\left(T_{gas} - T_{wall}\right) \quad (2)$$
- prescribing a radiative heat input at the inner wall using the CFD calculated maximum gas temperature (T_{max}) inside the liner. The radiative heat input is defined as
$$Q_{rad} = \sigma_{SB}\varepsilon^{*}\left(T_{\max}^{4} - T_{wall}^{4}\right) \quad (3)$$
where σ_{SB} is the Stefan-Boltzmann constant and ε^{*} is the emissivity of the wall. For a metal surface the value of ε^{*} is about 0.75. However, a ceramic Thermal Barrier Coating (TBC) was applied to the liner wall, reducing the emissivity to 0.35 [13].
- prescribing a wall adjacent gas temperature equal to the combustor inlet temperature and a heat transfer coefficient, obtained from the Nusselt correlation of Dittus-Boelter, at the outer wall of the liner (convective boundary condition, Q_{conv}).
- prescribing a radiative heat input at the outer wall using the casing temperature as T_{max}. It was assumed that the casing temperature is 100 K below the cooling gas temperature due to casing cooling from the outside.

Given these boundary conditions, the liner temperature distribution can be calculated.

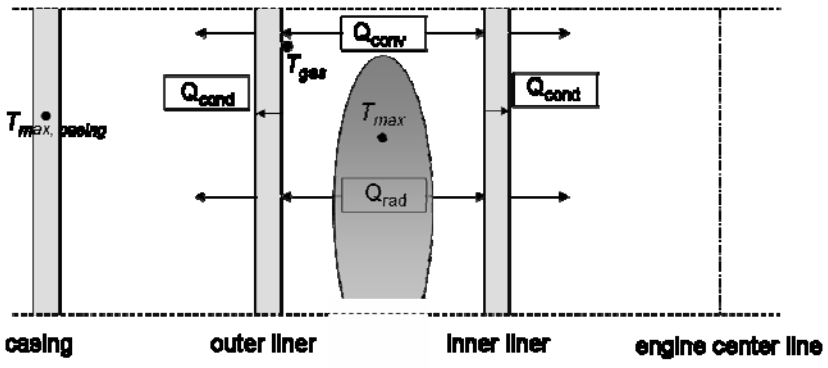

Figure 5 Schematic representation of heat flows in combustor cross section.

Before the CFD calculated temperature field could be applied as a boundary condition, it had to be transferred from the CFD grid to the FE mesh. The pre-processing program MSC.Patran was

used to transform the spatial fields for the CFD calculated temperature (T) and heat transfer coefficient (h) distribution to a convective FE nodal boundary condition.
The temperature drop across the TBC in the current application was approximated to be about five degrees in a steady-state condition. Since the effect is very limited, this aspect of the TBC was not taken into account in the analysis. The effect of a reduced emissivity has a larger influence on the thermal behavior and was therefore included in the model as was described before.

2.2.2 Structural analysis

Since only $1/16^{th}$ part of the liner was modeled, periodic boundary conditions were applied at the edges of the model to account for the constraints applied by the omitted part of the structure. Therefore displacements in circumferential direction were constrained at both end faces. Furthermore the rigid body motion was constrained by fixing one point of the model (on the lug near the attachment to the diffuser casing) in all three directions. Finally, at the down-stream end, both the inner and outer liner are fixed to the casing with metallic guides. These guides are sliding in axial direction and also provide some freedom to move in radial direction. Furthermore the guides are somewhat flexible, which means that after the offsets in radial and axial direction have been reached due to deformation of the liners, they are still not rigidly fixed in space. Since it was expected that the liner deformations would not exceed the offsets of the guides, no boundary conditions were applied in this region.
The temperature distribution as calculated in the thermal analysis were used as loading for the structural model. Due to differences in thermal expansion thermal stresses develop and the material deforms elasto-plastically.

2.3 Life assessment

Creep and low cycle fatigue (LCF) are the two potential failure mechanisms for a combustor liner. For both mechanisms a lifing method was defined as will be described in this section. Also the interaction between the mechanisms is discussed.
The creep strain accumulation was calculated during the FE analysis. The creep strain rate depended on stress σ (in Pa) and temperature T (in K) in the following way

$$\dot{\varepsilon}_{cr} = 3.48.10^{-20}\, e^{4.02.10^{-8}\sigma}\, e^{0.0211T} \qquad (4)$$

FE analysis of one flight provides the creep strain accumulation during that flight. However, analyzing the complete service life of a combustor in this way is computationally not feasible. Therefore, a method was defined to determine creep life based on a FE calculation of limited duration (Δt).

The most straightforward method is extrapolation of the damage after one flight (using the *average* creep rate) towards the critical amount of creep damage, also known as Robinson's rule:

$$t_{cr} = \frac{\varepsilon_{cr,critical}}{\varepsilon_{cr,\Delta t}} \Delta t = \frac{\varepsilon_{cr,critical}}{\dot{\varepsilon}_{cr,aver}} \quad (5)$$

where $\varepsilon_{cr,critical}$ is the creep strain that is associated with the end of life.
However, it is well known that creep is not a linear process. The first reason is the non-linear shape of the creep curve and the second reason is the occurrence of stress relaxation. This makes that the creep strain rate is initially very high but then decreases to a constant value. If a FE creep analysis is performed for one flight, only a small part of the creep curve is covered and the constant creep rate is not reached. Extrapolation with the *average* creep rate towards the critical creep strain then yields a (very) conservative estimate of the creep life. Therefore the *tangent* creep rate at the end of the time period ($\dot{\varepsilon}_{cr,\Delta t}$) was used for the extrapolation, which yields a less conservative life assessment.

$$t_{cr} = \frac{\varepsilon_{cr,critical}}{\dot{\varepsilon}_{cr,\Delta t}} \quad (6)$$

The value of $\varepsilon_{cr,critical}$ is typically 2% creep strain. Note that this value is lower than the creep strain at rupture. However, creep rupture does not occur in this situation, since at creep strains of 2% other failure mechanisms, like coating spallation or grain boundary oxidation become active and are the life limiting mechanisms.
For the low cycle fatigue (LCF) life analysis the cyclic loading of the construction is required. The relation between total strain range ($\Delta\varepsilon_{tot}$ in %) and LCF life (N_{LCF}) was obtained from Seeley et al. [12] and the functional relation used in the FE analysis is given by

$$N_{LCF} = \left(\frac{\Delta\varepsilon_{tot}}{21.253} \right)^{-2.36} \quad (7)$$

which represents the 870 ^{o}C curve.
For LCF conditions the load cycles contain both elastic and plastic deformation, which means that the LCF life is related to the total strain range ($\Delta\varepsilon_{tot} = \Delta\varepsilon_{el} + \Delta\varepsilon_{pl}$). Furthermore, it is generally accepted that the occurrence of cracks, and therefore the LCF life, is best correlated with the *maximum principal* strain component. Thus, the sequence of this strain component during the transient FE analysis is used to calculate the LCF life distribution in the combustor.
Finally it is possible to combine the creep and fatigue damage to obtain the total creep and fatigue life of the combustor. However, it is very difficult to obtain the proper interaction between the two failure mechanisms. The simplest method is to combine the two mechanisms linearly, which is known as the Miner - Robinson rule:

$$\frac{1}{N_{tot}} = \frac{1}{N_{LCF}} + \frac{1}{N_{cr}} \quad (8)$$

3 Analysis of a complete flight

The integrated approach described in the previous section can be used to analyse the liner loading and life consumption for a single operating condition. However, a real flight is a sequence of a large number of different operating conditions. Analysing all conditions separately is computationally not feasible. Therefore a method was developed to efficiently analyse a complete flight. In this section the method is described and the accuracy is demonstrated.

3.1 Method description

The basic idea of the method is that detailed CFD analyses were performed for a limited number of characteristic conditions and that for any other condition thermal input properties were obtained by interpolating between these conditions. The time scale of the processes in the combustor fluid domain (~ milliseconds) is very different from the time scale of the overall engine transients (~ seconds). The transient behavior of the engine (e.g. fast or slow accelerations) is captured by GSP and translated into time-sequences of the quantities that characterize the combustion process (fuel and airflow). Since the sampling rate of these quantities is in the order of seconds, it is appropriate to consider a transient mission analysis as a number of consecutive quasi-steady-state CFD analyses. Therefore there is no need to do transient CFD analyses.

Appropriate quantities for interpolation, interpolation functions and characteristic conditions had to be defined. Therefore a large number of measured flights were analysed with the gas turbine simulation program GSP. Air inlet temperature (TT3) and fuel / air ratio (W_f / W_{air}) proved to be the only two quantities required to fully characterise the combustor operating condition. Also the operating ranges of these parameters were established in this way, resulting in the definition of five characteristic operating conditions as indicated in Table 1. CFD analyses were performed for these five conditions and the results were stored in a database.

Table 1 Details of characteristic operating conditions.

Condition	1	2	3	4	5
TT3[K]	750	380	1000	750	750
Wf / W_{air}	0.0257	0.0257	0.0257	0.0033	0.0118

Interpolation functions were selected for the quantities required to define the boundary conditions in the FE analysis: wall adjacent gas temperature, inside heat transfer coefficient, maximum gas temperature and outside heat transfer coefficient. GSP analyses showed that the gas temperature rise in the combustor was almost directly proportional to the fuel / air ratio, but the

proportionality constant depended on the initial gas temperature value. Therefore the following linear interpolation function was adopted for the wall adjacent gas temperature.

$$T_{gas} = bTT3 + a\frac{W_f}{W_{air}} \quad \Leftrightarrow \quad \frac{T_{gas}}{TT3} = b + a\frac{W_f}{W_{air}TT3} \tag{9}$$

The heat transfer coefficient is largely determined by the amount of turbulence in the flow, which is strongly related to the mass flow. Therefore the following linear interpolation function was adopted for the heat transfer coefficient.

$$h = c + dW_{air} \tag{10}$$

The interpolation functions for the maximum temperature in the combustor (used for radiative heat input) and the outside heat transfer coefficient were defined as

$$T_{\max} = 925 + TT3 + 22946\frac{W_f}{W_{air}} \tag{11}$$

$$h_{outside} = 22.6 \cdot W_{air} \tag{12}$$

The parameters *a, b, c* en *d* in Eqs. (9) and (10) were determined for every node on the liner inner surface by fitting the functions to the five result cases that were available in the database of CFD results. This was done by using a least squares fitting method. The parameters were stored in a file, which was used during the transient FE analyses. The functions in Eqs. (11) and (12) are valid for the entire combustor model and therefore do not require fitting for all nodes.

The method to perform a transient analysis of a complete flight is shown schematically in Figure 6 and can be summarized as follows.

- A number of CFD analyses were performed for five characteristic engine operating conditions that span the operating range, see Table 1.
- The calculated wall adjacent temperature distribution and heat transfer coefficient distribution for these conditions were transformed to FE boundary conditions and stored in a database.
- A recorded flight is analyzed with GSP as a transient analysis. GSP calculates the time sequence of the input variables TT3 and W_f / W_{air}.
- A transient thermal FE analysis is performed in which the time-dependent boundary conditions are calculated by ***interpolating*** (for every node at the liner inner surface) between the conditions in the CFD database, based on the given values of TT3 and fuel / air ratio.
- A transient structural FE analysis is performed in which the calculated time-dependent temperature distribution is imposed as loading.
- A life assessment is performed based on the FE calculated stress and temperature sequences.

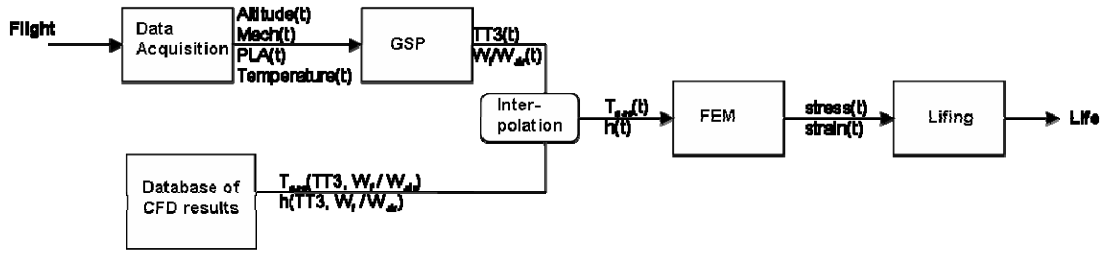

Figure 6 Schematic representation of mission analysis method.

3.2 Method validation

In addition to the five CFD analyses for the conditions given in Table 1, one extra CFD analysis was performed to validate the interpolation method. The condition of this analysis, referred to as condition 6, represents the engine design point characterized by $TT3$ = 817.6 K and W_f / W_{air} = 0.0322. This yields a fuel / air ratio of 0.0322 and a condition that is quite different from any of the other conditions in Table 1.

The first validation was done by comparing the CFD calculated T_{gas} and h with the interpolated T_{gas} and h. The result for every node on the liner inner surface is shown in Figure 7. This shows that for the gas temperature the average of the complete set of points is on the 1-to-1 line and the deviation from the calculated value is typically less than 10%. For the heat transfer coefficient the correlation is even better.

Another validation of the method is shown in Figure 8, where the calculated liner temperature distribution based on the CFD calculated and interpolated T_{gas} and h are compared. The distribution is very similar and also the global temperature values are very comparable. Only at the hot spots the interpolated temperature was in this case about 150 degrees higher. This is a considerable deviation, but it is only for a small number of local spots. That may imply that at those spots the stresses relax quickly and that the effect on life consumption is small. However, the exact influence of these temperature deviations on life consumption was not determined. Furthermore the condition used for validation is a severe condition which is quite different from the conditions used for interpolation. Therefore, for other conditions that occur during a mission the deviations may be smaller.

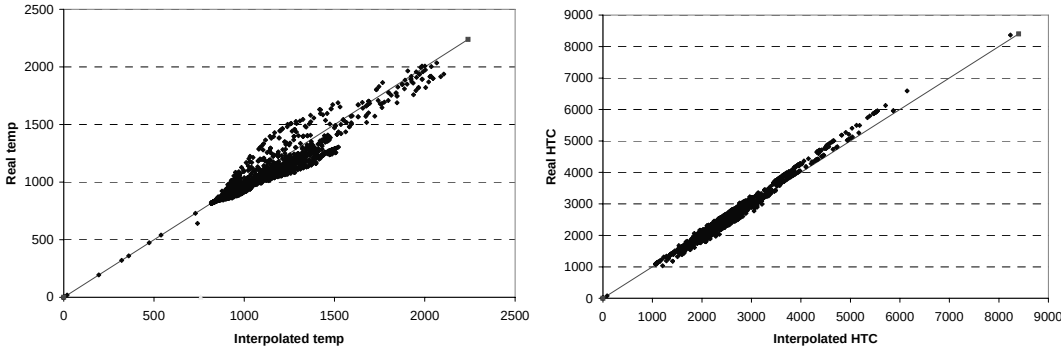

Figure 7 Comparison of CFD calculated and interpolated T_{gas} and h.

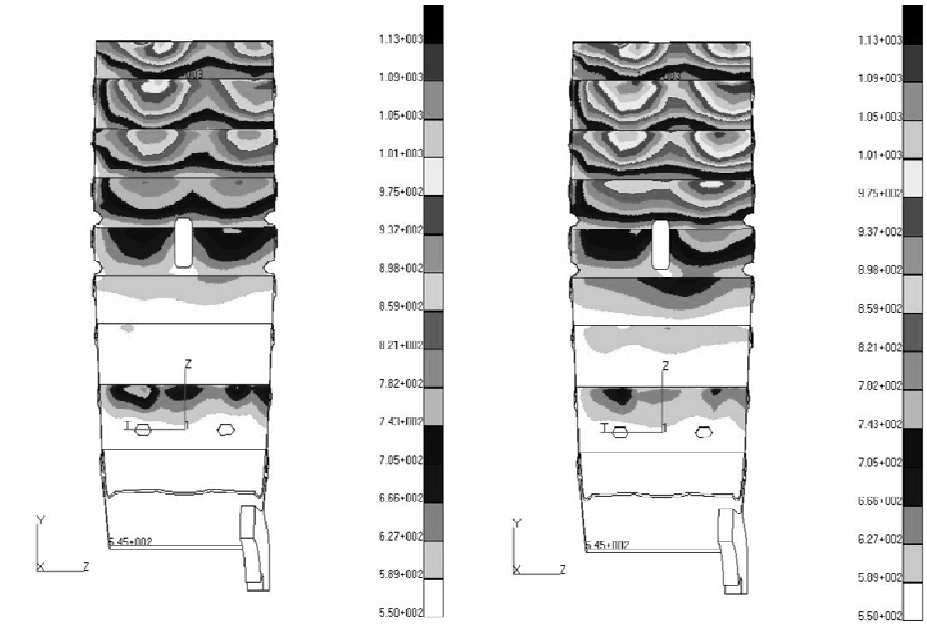

Figure 8 Comparison of results based on real (left) and interpolated temperature distribution on outer liner.

These two validation cases show that the method developed reduced the computational effort for a mission analysis enormously and still retained a very acceptable accuracy level. If a higher accuracy is required, the number of CFD analyses can be extended, which improves the interpolation method. However, the consequence will be a more time-consuming and more costly analysis.

4 Results

The integrated approach as described in section 2 and 3 was used to analyse a real flight and perform a combustor liner life assessment. The variation of power setting (PLA) and flight altitude for the selected flight are shown in Figure 9. The analysis results are shown in this section, starting with the flow properties predicted by the CFD analysis for a selected condition. Then the predicted temperature and stress distribution are shown and the results of the life assessment are presented. Finally the results were compared to the damage observed in practice to validate the approach.

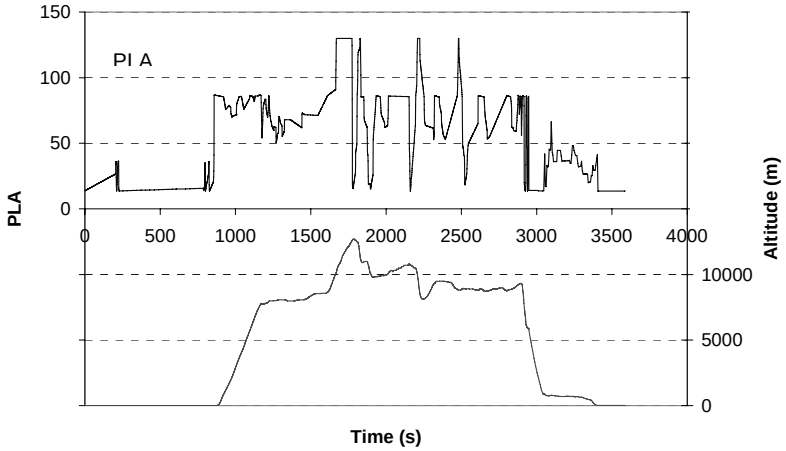

Figure 9 Variation of power setting (PLA) and flight altitude during analyzed mission.

4.1 Flow properties

Figure 10 shows a vector plot of the flow field in a radial cross-section of the burner for the first of the characteristic operating conditions (condition 1, see Table 1). As a result of the swirling inlet flow, a recirculation zone is established, providing flame stabilisation. This recirculation zone is noticed by reversing flow near the burner outlet. Additionally, since the cross-section is made in the plane of the boroscope hole, the effect of the cooling air flowing through this hole is clearly seen.

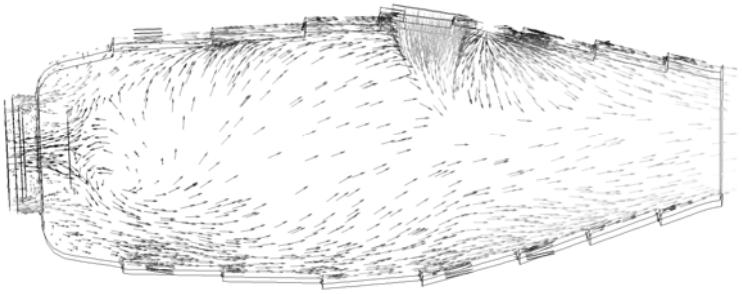

Figure 10 Vector plot of the velocity field in a radial plane of the combustor.

A contour plot of the scaled temperature field at the same operating condition is displayed in Figure 11. The cooling air that is introduced by the boroscope hole is clearly influencing the temperature field. Moreover, due to the applied film cooling, the fluid near the wall remains relatively cool. The maximum temperature is found at approximately halfway the length of the combustor.

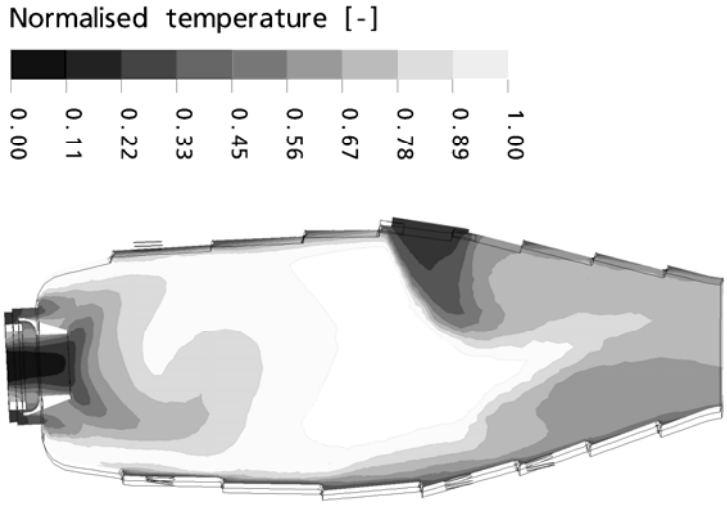

Figure 11 Contour plot of the temperature field in a radial plane of the combustor at condition 1.

4.2 Thermal and structural results

The temperature distribution in the liner walls at operating condition 6 is shown in Figure 12a. This shows that the thermal loading of the liner is maximum at the down-stream end of the inner liner. Figure 12b shows the tangential stress distribution in the liner walls. As with the temperature, the extreme values were found at the down-stream ends of inner and outer liner.

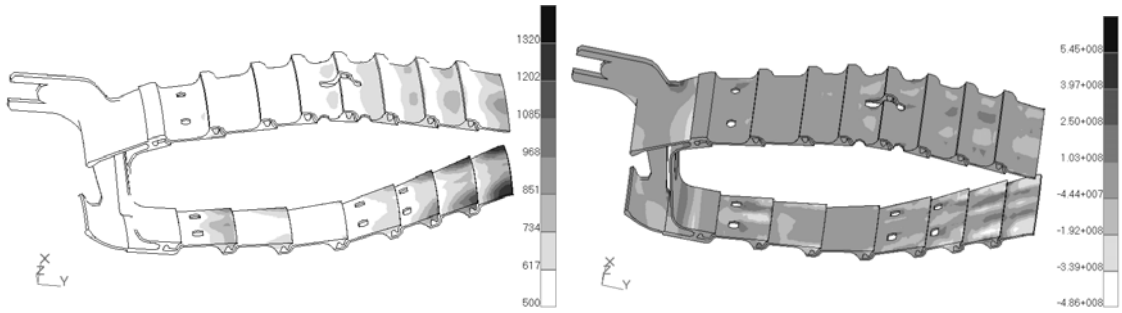

a) *b)*

Figure 12 a) temperature (in ^{o}C) and b) tangential stress (in Pa) distribution at operating condition 6.

The time-variation of temperature and stress during the complete flight for the four locations indicated in Figure 13 is shown in Figure 14. This shows that significant variations in temperature and stress occur during the flight. For locations on the inside of the liners, stresses were mainly compressive, whereas locations on the outside were in a tensile stress state. However, the situation can be completely opposite at fast transients, as is observed just after 2000 s. Also, the average stress level decreased during the flight, which is caused by stress relaxation due to creep.

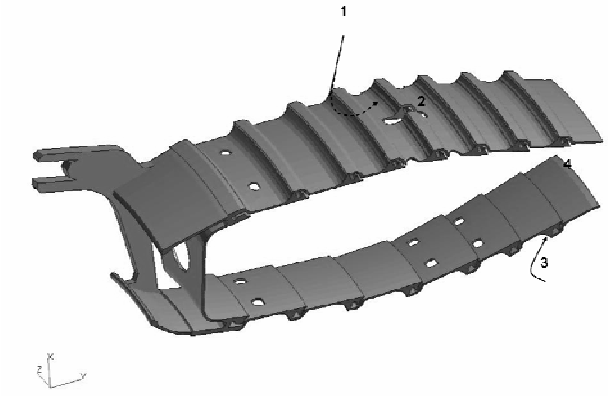

Figure 13 Location of nodes used for plotting the temperature and stress history.

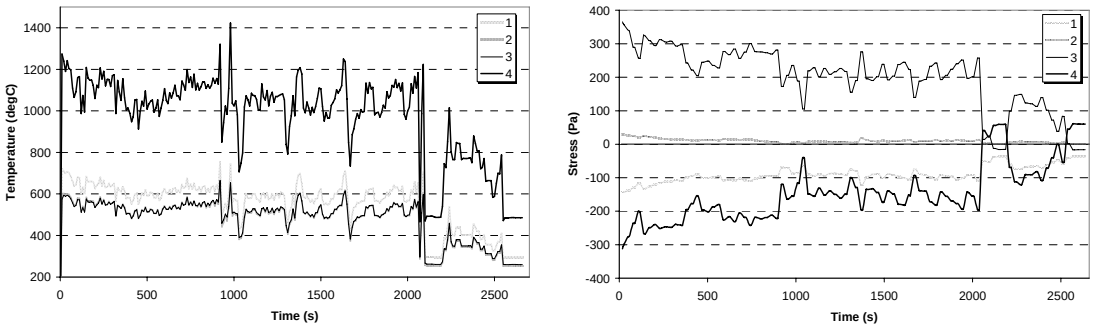

Figure 14 Temperature and tangential stress variation on liner during a mission for the locations shown in Figure 13.

4.3 Life assessment

The temperature and stress history were used to perform a life assessment on the combustor liner. Both the creep life and low cycle fatigue life were calculated applying the methods described in section 2.3. The calculated distribution of creep and LCF life are shown in Figure 15, indicating the critical locations on the liners. This plot shows that the creep life is minimal at the final louvers of both inner and outer liner with a minimum value of only 4 hours. This calculated life is much too low and is probably a result of an overestimated temperature in the liner. Since the creep mechanism is extremely sensitive to the temperature, a small deviation in temperature leads to significant changes in creep life. This problem in predicting the creep life is a result of the lack of accuracy in the prediction of absolute values that will be addressed in the next subsection.

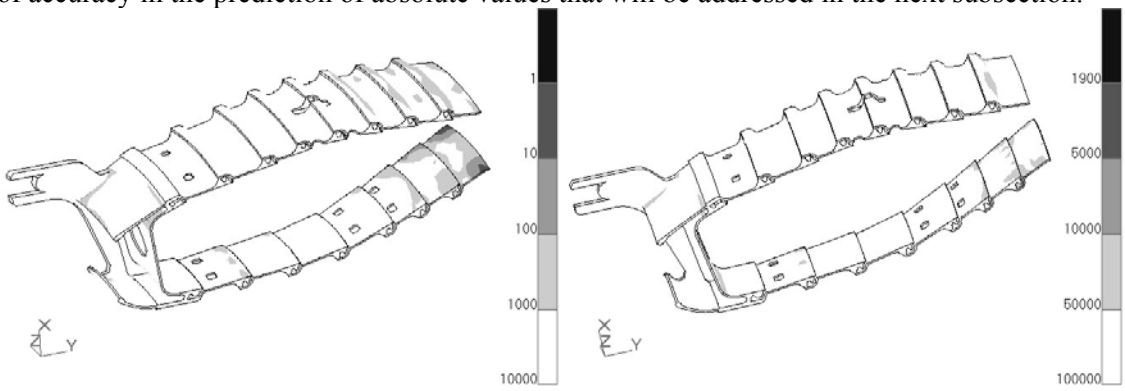

Figure 15 Creep life (in hrs) and fatigue life (in # flights) distribution in the liner.

The minimum calculated fatigue life is around 1900 flights at some very small areas, mainly at the final louvers of the inner and outer liner. The majority of the structure has a fatigue life well above 10000 flights.

4.4 Model validation

To gain insight in its predictive capability the model had to be validated, especially because a large number of assumptions and approximations were made in the CFD, FE and lifing analyses. Ideally, the model should have been validated and tuned to experimental data after each step in the sequence. For example, detailed information about the temperature distribution in the liner at a specific operating condition would give the possibility to tune the values of the outside heat transfer coefficients to obtain a good correlation with the available data. However, experimental data to do so was not available. Actually, the only way to validate the model was to compare the calculated life to the values observed in practice. This means that in the very complex chain of CFD - FE thermal - FE structural - life assessment analyses no intermediate check of the model was possible. It is quite likely that some assumption somewhere in one of the analyses lead to a deviation in results.

The results of the life assessment were compared to the damage observed in practice as shown in Figure 1. The location of crack initiation is expected to coincide with the location of lowest calculated fatigue life. As can be seen in Figure 15, the lowest fatigue life was calculated at the final three louvers of the inner and outer liner. Furthermore the creep damage on the final three louvers of the inner liner is significantly higher than on those of the outer liner. Since creep is believed to enhance crack initiation, it may be concluded that cracks will start to initiate at the final three louvers of the inner liner. This correlates well with the observation in practice that cracks initiate at the inner liner on the 4^{th} to 9^{th} louver.

The direction of crack growth is related to the orientation of the stress tensor in the material. In other words, cracks propagate mainly in a direction perpendicular to the maximum principal stress. Comparison of the different components of the calculated stress distribution in the louvers showed that the circumferential stress was the largest stress component and also best resembled the max principal stress distribution, as is shown in Figure 16. This means that cracks will propagate in axial direction, as was observed in practice.

Finally the number of cycles / flights to fatigue crack initiation could be checked. This showed that the order of magnitude of the calculated life corresponded to the real life, but the absolute prediction is not very accurate.

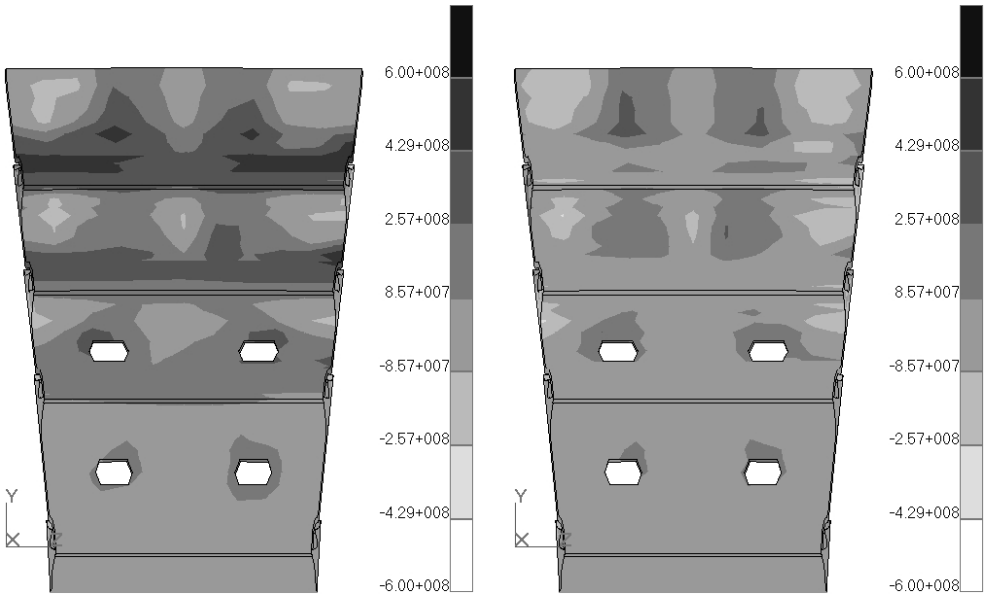

a) *b)*

Figure 16 Distribution of a) circumferential and b) max. principal stress on the final louvers of the inner liner.

The only proper way to improve the predictive capability of the model is validation of intermediate results with experimental data. Although the prediction of absolute values for combustor life at certain operating conditions is hard, the current method is very appropriate to perform comparative life assessments. In that case a wrong assumption somewhere in the model has a similar effect for every condition that is analyzed, which reduces the inaccuracy of the *comparison* considerably. Examples of such analyses are comparison of different mission types in terms of life consumption or the effect of increased firing temperature (due to compressor or turbine deterioration) on life consumption.

5 Conclusions

The following conclusions can be drawn from this work:

- The results of a CFD analysis were successfully linked to a FE model, which gave the possibility to calculate the thermal loading of the combustor for an arbitrary operating condition.
- An efficient method was developed to analyze a complete measured flight. A compromise between accuracy and computational effort must be found for each application.
- Although the actual number of cycles to crack initiation could not be predicted accurately, the location of crack initiation and the direction of crack growth correlated well to the observations in practice.
- The developed models and tools can be applied to perform comparative life assessment, e.g. for different mission types.

6 References

[1] Walls, D.P., deLaneuville, R.E., 1997, "Damage Tolerance Based Life Prediction in Gas Turbine Engine Blades under Vibratory High Cycle Fatigue", J. Engineering for Gas Turbines and Power, 119, 143-146.

[2] Harrison, G.F., Tranter, P.H., 1995, "Modelling of Thermomechanical Fatigue in Aero Engine Turbine Blades", AGARD Conf. Proc. 569, paper no. 16.

[3] Tinga, T., Visser, W.P.J., de Wolf, W.B., and Broomhead, M.B.J., 2000, "Integrated Life Analysis Tool for Gas Turbine Components", ASME paper 2000-GT-646, NLR-TP-2000-049.

[4] Scott Crocker, D., Nickolaus, D., and Smith, C.E., 1998, "CFD Modeling of a Gas Turbine Combustor from Compressor Exit to Turbine Inlet", ASME paper 98-GT-184.

[5] Sivaramakrishna, G., Muthuveerappan, N., Venkataraman, S., and Sampathkumaran, T.K., 2001, "CFD Modeling of the Aero Gas Turbine Combustor, ASME paper 2001-GT-0063.

[6] Malecki, R.E., and Rhie, C.M., 2001, "Application of an Advanced CFD-Based Analysis System to the PW6000 Combustor to Optimize Exit Temperature Distribution - Part I: Description and Validation of the Analysis Tool", ASME paper 2001-GT-0062.

[7] McQuirk, J.J., and Spencer, A., 2000, "Coupled and Uncoupled CFD Prediction of the Characteristics of Jets from Combustor Air Admission Ports, ASME paper 2000-GT-125.

[8] Snyder, T.S., Stewart, J.F., Stoner, M.D., and McKinney, R.G., 2001, "Application of an Advanced CFD-Based Analysis System to the PW6000 Combustor to Optimize Exit Temperature Distribution - Part II: Comparison of Predictions to Full Annular Rig Test Data", ASME paper 2001-GT-0064.

[9] Fuller, E.J., and Smith, C.E., 1993, "Integrated CFD Modeling of Gas Turbine Combustor", AIAA paper 93-2196.

[10] Lai, M.K., 1997, "CFD Analysis of Liquid Spray Combustion in a Gas Turbine Combustor"; ASME paper 97-GT-309.

[11] Kiewel, H., Aktaa, J., and Munz, D., 2002, "Advances in the Inelastic Failure Analysis of Combustor Structures", in: High Intensity Combustors - Steady Isobaric Combustion, Final Report of the Collaborative Research Centre 167, Wittig, S., and Vohringer, O., eds., Wiley-VCH, Weinheim.

[12] Seeley, R.R., and Ishwar, V.R., 1999, "Fatigue in Modern Nickel-base Alloys for Gas Turbine Applications", Proc. Conf. Life Assessment of Hot Section Gas Turbine Components, Edinburgh, UK.

[13] Wittig, S., Vohringer, O., 2002, "High Intensity Combustors - Steady Isobaric Combustion", Final Report of the Collaborative Research Centre 167, Wittig, S., and Vohringer, O., eds., Wiley-VCH, Weinheim.

[14] Visser, W.P.J., and Broomhead, M.J., 2000, "GSP - A Generic Object-Oriented Gas Turbine Simulation Environment", ASME paper 2000-GT-002, NLR-TP-2000-267, www.gspteam.com.

[15] De Jager, B., Kok J.B.W. and Van der Meer, Th.H. , "Development of reduced chemistry with CSP for application in turbulent n-Heptane flames", Proceedings of the European Congress on Computational Methods in Applied Sciences and Engineering (ECCOMAS), P. Neittaanmäki, T. Rossi, K. Majava, and O. Pironneau (eds.) W. Rodi and P. Le Quéré (assoc. eds.), Jyväskylä, July 24 – 28, 2004.

[16] Williams, F.A., 2003, Technical report, http://maemail.ucsd.edu/combustion/cermech/.

[17] Rupley, F.M., Kee, R.J. and Miller, J.A., "Chemkin II: A FORTRAN chemical kinetics package for the analysis of gasphase chemical kinetics"

[18] Goussis, D.A., and Lam, S.H., 1994, "The CSP Method for Simplifying Kinetics", Int. Journal of Chem. Kin, 26, pp. 461–486.

[19] Mastorakos, E., Massias, A., Diamantis, D., and Goussis, D.A., 1999, "An Algorithm for the Construction of Global Reduced Mechanisms with CSP Data", Combustion and Flame, 117, pp. 685–708.

[20] Varatharajan, B., Li, S. C., and Williams, F. A., 2001, "The Chemistry of JP10 Ignition, AIAA Journal, 39(12), pp. 2351–2356.

Appendix A JP10 jet fuel chemistry

JP10 is a hydrocarbon fuel that is used in aero gas turbines. The molecule consists of 10 C atoms and 16 H atoms and its systematical name is Tricyclo[5.2.10]decane. Stoichiometric oxidation is given by the reaction

$$C_{10}H_{16} + 14O_2 \rightarrow 8H_2O + 10CO_2$$

Williams et al. [16],[17] provided a mechanism for the oxidation of JP10 that consists of 42 species and 201 reactions. The basis of this mechanism is the San Diego Combustion mechanism. Added to this mechanism is a mechanism for the combustion of JP10. This addition consists of the break-up of the JP10 molecule into smaller hydrocarbons like butadiene etc.
Laminar premixed 1D flame calculations at atmospheric and elevated pressure yielded insight in the chemical reactions that dominate the oxidation behavior of JP10. The laminar flame calculations were analyzed using the Computation Singular Perturbation (CSP) [18] technique, in order to select dominant species that govern the conversion of JP10 into products. This CSP analysis can give a global reaction rate as a function of the species in the mechanism or temperature.

Laminar flames

Insight in the global rates can be obtained by simulating a laminar premixed flame. In this report the results of a stoichiometric flame at 1 atm and 18 atm are shown. Figure A1 shows that the mechanism is behaving differently at atmospheric and high pressure. The temperature profile of the laminar flame at atmospheric pressure has a less steep descent than the temperature profile at 18 atm. The concentration of intermediate species and combustion products is not changing very much with the different pressures.

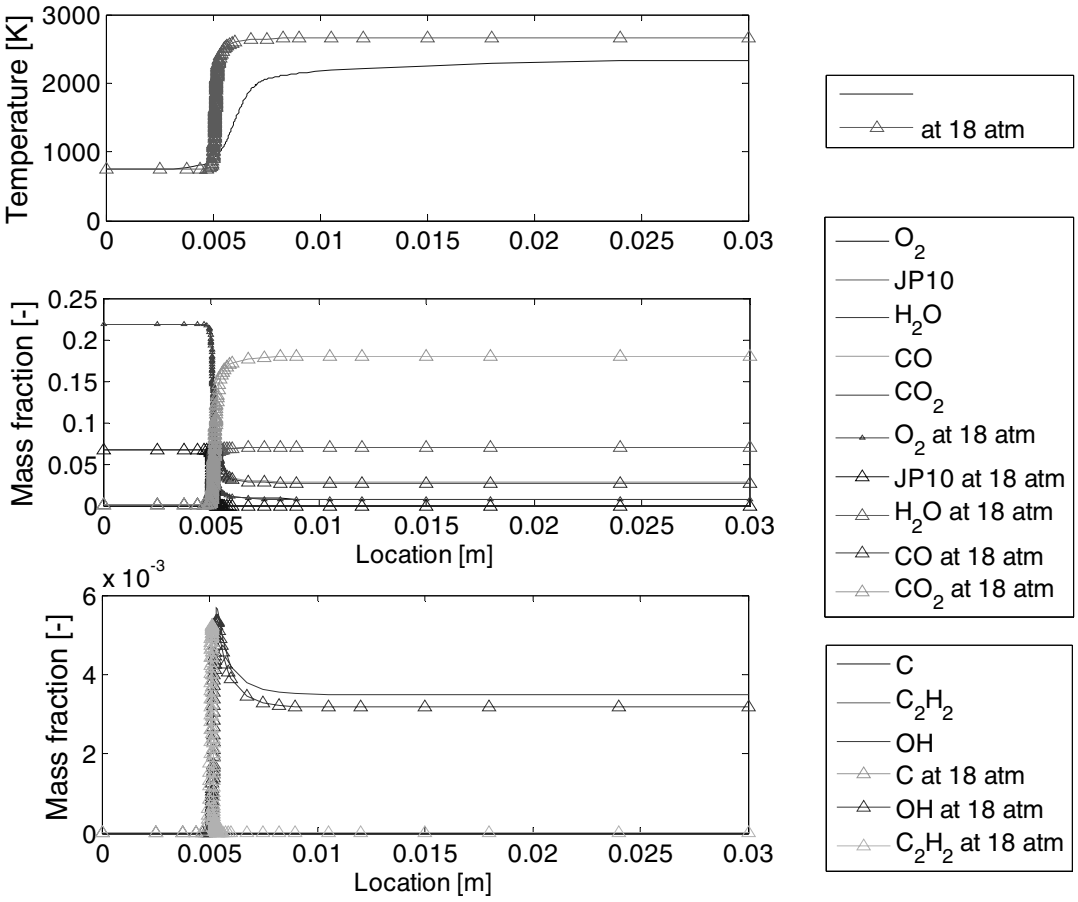

Figure A1 The temperature and species profiles for a premixed flame at a pressure of 1 and 18 atm.

CSP reduction

CSP analysis was carried out using the results from the laminar flame. A theoretical background of this method can be found in papers by Goussis et al. [18][19]. This analysis yields the species in Table A1 to be dominant in reaction rate determination, if the mechanism is to be projected on one global step. The global step that is constructed by CSP is given by the following reaction

$$CO_2 \rightarrow CO + O_2$$

The results from CSP are similar to reduction of methane combustion as is reported by Diamantis et al. [19]. An explanation for this is that both methane and JP10 are hydrocarbons and globally the same type of CH bond needs to be broken. Other types of CH bonds are also present in the JP10 mechanism, but they do not seem to affect the global step. The global step is not a physical step, it can rather be seen as an overall reaction that yields from element and mass conservation, but with *virtual* species.

Table A1 Non steady-state species

CO	CO_2	O_2	H_2O	N_2	AR

Rate fitting and turbulent simulations

Using the CSP analysis it is possible to construct a global reaction rate, that represents the overall oxidation process composed of steady state relations. This composed reaction rate is accompanied by a composed species η that represents the thermo-chemical state of the mixture. In Figure A2 this CSP analysis is projected on the laminar flame results from the previous section. It is seen that for atmospheric and high pressure there is a significant difference in the concentration profile of η. At high pressure the composed species behaves as a fuel molecule: a high initial concentration and during ignition a high consumption rate of the composed species. The shape of this profile is similar to the JP10 concentration profiles in Figure A1. For atmospheric pressure, the composed species concentration profile is not showing much resemblance with a fuel molecule.

For turbulent combustion simulations the composed species and global rate can be used as a single step mechanism. This gives the advantage that only one extra transport equation is needed. From the laminar flame data at 18 atm the reaction rate as a function of temperature is known. In order to establish an Arrhenius like relation for the global conversion of JP10 into combustion product, a Gaussian fit can be applied to this data (see Figure A3). The Gaussian function is given by

$$S_\eta = 2610 e^{-\left(\frac{T-1938}{358.2}\right)} \ [kg/m^3/s] \qquad (13)$$

This fitted rate can be used in a simple finite rate combustion simulation.

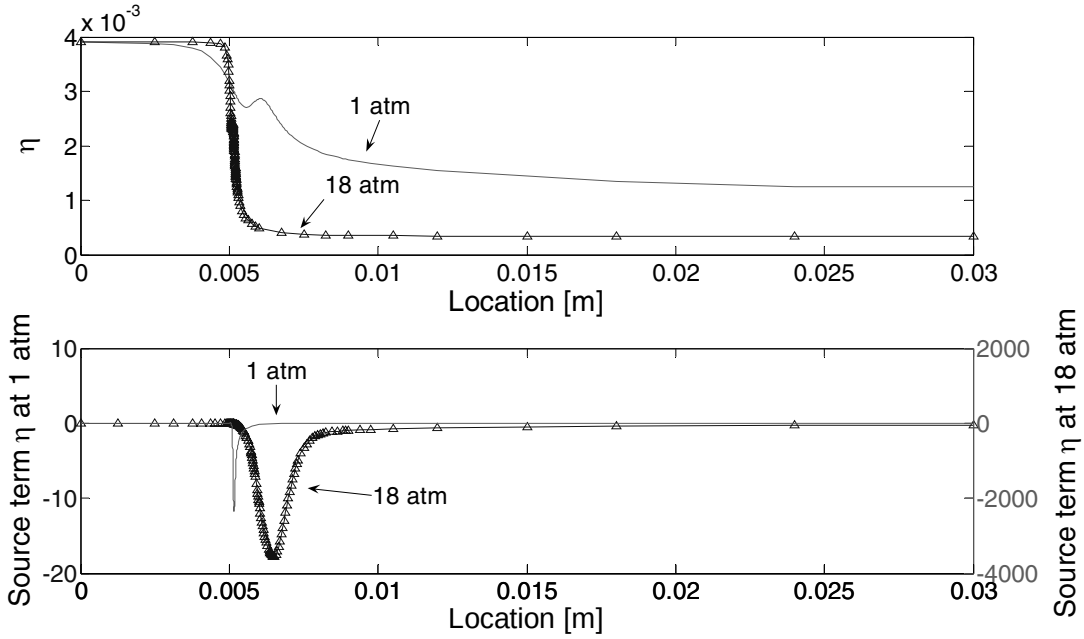

Figure A2 Composed species concentration and source term (reaction rate)

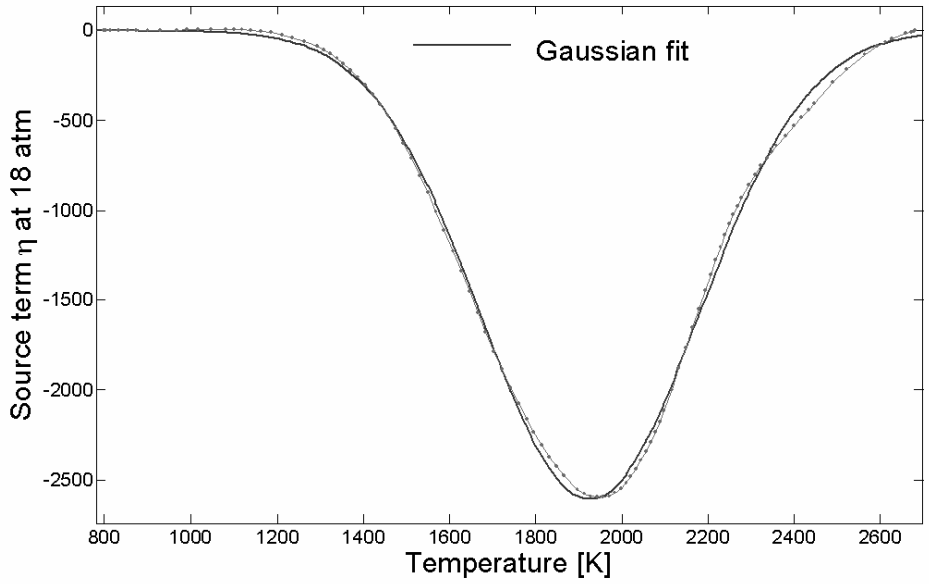

Figure A3 CSP source term (reaction rate) fitted with Gaussian function.